

Novel Curcumin-Diethyl Fumarate Hybrid as a Dualistic GSK-3 β Inhibitor/Nrf2 Inducer for the Treatment of Parkinson's Disease

Rita Maria Concetta Di Martino,¹ Letizia Pruccoli,¹ Alessandra Bisi, Silvia Gobbi, Angela Rampa, Ana Martinez, Concepción Pérez, Loreto Martinez-Gonzalez, Maria Paglione, Elia Di Schiavi, Francesca Seghetti, Andrea Tarozzi,* and Federica Belluti*

Cite This: *ACS Chem. Neurosci.* 2020, 11, 2728–2740

Read Online

ACCESS |

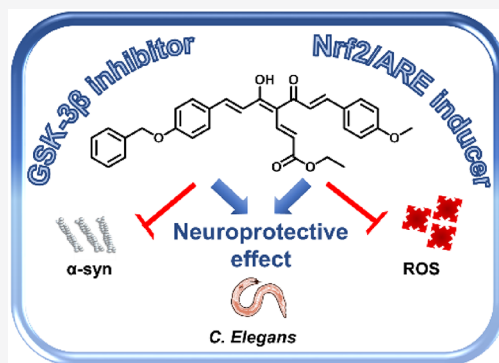
 Metrics & More

 Article Recommendations

 Supporting Information

ABSTRACT: Common copathogenic factors, including oxidative stress and neuroinflammation, are found to play a vital role in the development of neurodegenerative disorders, including Alzheimer's disease (AD) and Parkinson's disease (PD). Nowadays, owing to the multifactorial character of the diseases, no effective therapies are available, thus underlying the need for new strategies. Overexpression of the enzyme GSK-3 β and downregulation of the Nrf2/ARE pathway are responsible for a decrease in antioxidant defense effects. These pieces of evidence underline the usefulness of dual GSK-3 β inhibitors/Nrf2 inducers. In this regard, to design a dual modulator, the structures of a curcumin-based analogue, as GSK-3 β inhibitor, and a diethyl fumarate fragment, as Nrf2 inducer, were combined. Among the hybrids, **5** and **6** proved to effectively inhibit GSK-3 β , while **4** and **5** showed a marked ability to activate Nrf2 together to increase the neuronal resistance to oxidative stress. These last pieces of evidence translated into specific neuroprotective effects of **4** and **5** against PD pathological events including neurotoxicity elicited by α -synuclein aggregates and 6-hydroxydopamine. Hybrid **5** also showed neuroprotective effects in a *C. elegans* model of PD where the activation of GSK-3 β is intimately involved in Nrf2 regulation. In summary, **5** emerged as an interesting multitarget derivative, valuable to be exploited in a multitarget PD perspective.

KEYWORDS: Curcumin analogues, Diethyl fumarate, Neurodegeneration, Nuclear factor-erythroid related factor 2, Glycogen synthase kinase-3 β , Oxidative stress, Parkinson's disease



INTRODUCTION

Neurodegenerative diseases (NDDs) such as Alzheimer's disease (AD), Huntington's disease, Parkinson's disease (PD), and amyotrophic lateral sclerosis are increasingly recognized as major causes of death and disability worldwide.¹ They are characterized by a progressive impairment of cognitive and/or motor functions that reflect the loss of specific neurons in distinct central nervous system (CNS) regions.²

Although AD and PD, the two most common NDDs, show different clinical profiles, common molecular pathogenic mechanisms including oxidative stress, proteostasis, mitochondrial deficit, glutamate excitotoxicity, and neuroinflammation are observed in both diseases, suggesting converging pathways of neurodegeneration.³

In particular, oxidative stress is implicated in the proteostasis phenomena and leads to misfolding of neurotoxic proteins such as α -synuclein (α -syn) in Lewy bodies (LBs) of PD and phospho-tau (p-tau) and amyloid- β (A β) in neurofibrillary tangles and senile plaques, respectively, of AD.⁴

In this regard, there are several strategies for reducing the toxic effects of α -syn and p-tau targeting the different

proteostasis pathways.⁵ Among the shared pathogenic pathways, the dysregulation of the glycogen synthase kinase-3 β (GSK-3 β)/nuclear factor-erythroid related factor 2 (Nrf2) signaling pathway is implicated in the oxidative stress defenses in both AD and PD.⁶ Nrf2 plays an important role in antioxidant mechanisms in response to oxidative stress: in basal conditions, it is bound to its endogenous inhibitor Kelch-like ECH associated protein1 (Keap1), a cysteine-rich zinc-metalloprotein, involved in promoting Nrf2 degradation. In response to stress insults, such as reactive oxygen species (ROS), this factor is released from Keap1, and upon translocation to the nucleus, it binds to the antioxidant response element (ARE). The Keap1/Nrf2/ARE complex directly regulates the expression of some phase II detoxifying

Received: June 11, 2020

Accepted: July 14, 2020

Published: July 14, 2020



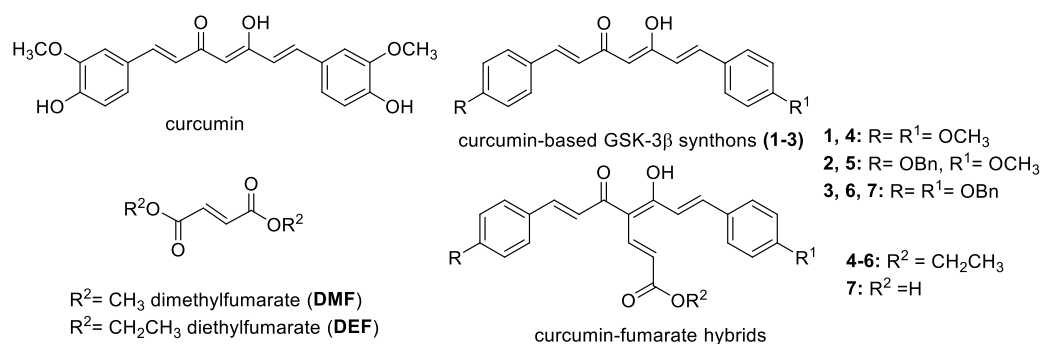


Figure 1. Chemical structures of curcumin and general structures of curcumin-based starting synthons (1–3), fumaric acid esters (DMF and DEF), and curcumin-fumarate hybrids (4–7).

enzymes and antioxidant stress genes, namely NAD(P)H: quinone oxidoreductase 1 (NQO1), heme oxygenase-1, glutathione S-transferase, and aldo-keto reductase.⁷ Further, Nrf2 ameliorates the inflammation response by inhibiting the translocation of nuclear factor- κ B (NF- κ B) and activating anti-inflammatory genes.^{8,9} An altered expression of Nrf2 in both neurons and astrocytes of PD and AD patients has been observed. More recent studies suggest that Nrf2 activation reduces α -syn and p-tau levels, facilitating the degradation of these toxic proteins through autophagy.^{10–12} Thus, the Nrf2 signaling cascade, as a valuable defense against oxidative stress insults and loss of proteostasis, has been recognized as a validated target for the development of therapeutics for PD and AD treatment.

The enzyme GSK-3, a multifunctional serine/threonine kinase, exists in two isoforms, i.e., GSK-3 α and GSK-3 β , and participates in a wide range of cellular processes and signaling pathways; its increased expression and activity have been observed in several NDDs including AD and PD. In particular, GSK-3 β , represents a determining factor for abnormal tau protein phosphorylation and aggregation into neurofibrillary tangles. In PD, elevated levels of hyperphosphorylated tau were also associated with high levels of insoluble α -syn, underlying the pivotal role of the α -syn/p-tau/GSK-3 β pathway. These events culminated in extensive oxidative stress and neuronal cell death.¹³ Regarding the functional aspects, this kinase is regulated by post-translational phosphorylations at Ser9 and Tyr216, associated with enzyme inhibition and activation, respectively. Moreover, activated GSK-3 β plays a pivotal role in the downregulation of Nrf2 through direct phosphorylation of Nrf2 that, in turn, promotes proteasomal degradation of Nrf2 in a Keap1-independent manner.¹⁴ Definitively, the inverse correlation between the aberrant activation of GSK-3 β and the downregulation of Nrf2, with a corresponding decrease of antioxidant gene expression and cell defense effects, reinforces the usefulness of GSK-3 β inhibition in achieving therapeutic benefit.⁴

The complex pathological mechanisms characterizing NNDs prompted consideration of polypharmacology as the most appropriate therapeutic approach by which to accomplish an effective and disease-modifying outcome. In particular, by modulating several targets involved in pathology, multitarget drugs could offer the possibility of attaining improved effectiveness compared to a single-target drug.^{15,16} In this complex framework, the negative correlation between GSK-3 β and Nrf2 suggests that small molecules joining GSK-3 β inhibition to Nrf2 induction could be valuable drug candidates for NDDs.¹⁷ The modulation of these targets, involved in the

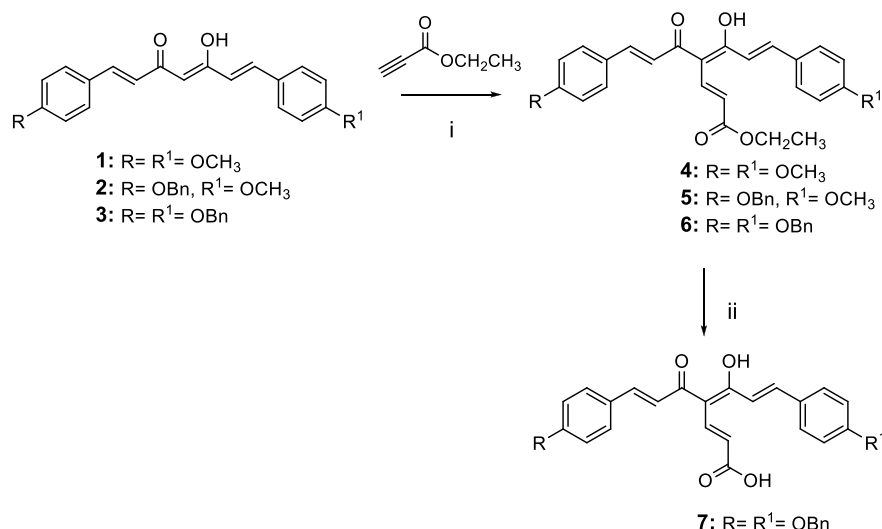
same signaling pathways in a feed-forward manner, could likely make it possible to obtain superior beneficial effect by reducing possible compensatory mechanisms and eliciting synergistic outcomes. Identifying chemical tools able to treat oxidative stress and inflammation, through the concomitant modulation of Nrf2 and GSK-3 β , could allow shedding light into this crucial cross talk.

Curcumin (Figure 1), the most abundant component of *Curcuma longa* rhizome, has gained considerable interest due to its pleiotropic therapeutic profile.¹⁸ At the molecular level, naturally occurring curcuminoids proved to modulate a large variety of interconnected pathways implicated in the pathogenesis of several multifactorial diseases such as cancer and NDDs.¹⁹ The capability of regulating the mediators and biological targets of the inflammation cascade contributes to this therapeutic effect.²⁰ In this respect, this natural compound, regarded as privileged structure, furnished the scaffold for the design of a large number of functionalized curcumin-based analogues endowed with significant antineurodegenerative activities, thus corroborating the enormous potential of this template in drug discovery.²¹

Several drawbacks have been reported for curcumin including poor solubility and chemical and metabolic instability that, in turn, negatively affect pharmacokinetic/pharmacodynamic properties, mainly ascribed to the 3-methoxy-4-hydroxy substitution pattern of the side aryl moieties. Moreover, curcumin and a variety of biologically active natural compounds, among them epigallocatechin gallate, mitoxantrone, resveratrol, and rifampicin, have been classified as pan-assay interfering compounds (PAINS) as they can generate false assay signals.^{22,18} Nevertheless, it is a widely shared opinion that compound reactivity might be dependent on the structural context; thus, properly designed molecules containing a PAINS-based structural motif can behave as selective modulators of some well-defined targets rather than reactive chemicals.^{23,24} This statement is strongly sustained by a large number of publications reporting bioactive curcumin-related molecules obtained upon adequate modification of the main framework, as documented by review articles.^{21c}

RESULTS AND DISCUSSION

Design Strategy of Curcumin-DEF Hybrids as Dual GSK-3 β /Nrf2 Modulators. GSK-3 β and Nrf2 could be regarded as valuable targets for NDDs treatment; their concurrent modulation through multitarget agents could offer promises for obtaining an improved therapeutic outcome associated with fewer undesirable side effects. Thus, the design of chemical entities endowed with the capability to

Scheme 1^a

^aReagents and conditions: (i) NaH, dry THF, 0 °C to rt, N₂, overnight, 41–84% yield; (ii) KOH (2 N CH₃OH solution), CH₃OH, 60 °C, 12 h, 75% yield.

concurrently interact with Nrf2 and GSK-3 β is a challenging task.

Several natural compounds endowed with an electrophilic motif, a well-established Michael acceptor system, proved to activate the Nrf2 pathway;²⁵ in particular, curcumin and fumaric acid esters (FAEs), i.e., dimethyl fumarate (DMF), were reported to covalently bind crucial cysteine residues of Keap1.²⁶ In a previous study, aimed at identifying new disease-modifying AD drug candidates, a small library of curcumin-based analogues was developed, leading to the identification of some active and balanced dualistic inhibitors of the enzymes β -secretase (BACE-1) and GSK-3 β also able to induce the antioxidant and anti-inflammatory enzyme NQO1. In line with this, aimed at designing new chemical entities as dual Nrf2 and GSK-3 β modulators, the previously identified GSK-3 β inhibitors 1–3 (Figure 1, IC₅₀ = 0.53, 2.78, and 2.49 μ M, respectively), chemically characterized by combinations of benzyloxy and methoxy substituents on the side aryl functions of the curcumin scaffold,^{21b} were selected as the starting platform for a hybridization strategy consisting of the introduction of a diethyl fumarate (DEF) fragment at the 4-position of the heptadienone framework.²⁷

Chemistry. The synthetic strategy for obtaining the curcumin-fumarate hybrids (4–7) is outlined in Scheme 1. The reaction of the starting synthons 1–3 with ethylpropiolate by using NaH as a base gave the corresponding analogues 4–6. The ethyl ester function of 6 was converted into an acidic function by treatment with KOH, to obtain 7.

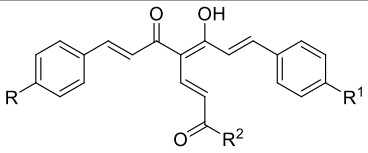
Biological Evaluations. The newly synthesized compounds (4–7) were studied for their anti-NDD potential, namely the capability to affect Nrf2 and GSK-3 β activities, along with the protective effect against a neurotoxic insult. In this context, a screening pipeline was followed. First, their inhibition of the GSK-3 β enzyme was evaluated by using a Luminescent Kinase Assay based on the quantification of the amount of the ATP present after the kinase reaction. In parallel, the neurotoxic effects of compounds 4–7 were evaluated in human neuronal cells (SH-SY5Y) in order to define the range of concentrations to be employed in the experimental setting. The most promising compounds were

studied for their indirect antioxidant effect (ability to modulate the Keap1/Nrf2/ARE pathway) upon assessment of their capability to induce glutathione (GSH) release and to decrease intracellular ROS formation under oxidative stress. In this regard, we used DMF as a positive control due to its known ability to mediate the antioxidant cellular defense by Nrf2 activation.²⁶ Afterward, analogues endowed with this property were selected to be evaluated for Nrf2 activation in terms of translocation of Nrf2 from the cytosol to the nucleus, Nrf2/ARE binding, and transcriptional activity. To achieve critical evidence regarding the therapeutic context of the tested compounds, namely AD or PD, studies on the protective effects against specific toxic insults by A β _{1–42} oligomers and 6-hydroxydopamine (6-OHDA) were performed. The effect of 4 and 5, characterized, among the series, by the more potent counteracting effects against 6-OHDA stimulus, was also investigated for their effect on α -syn aggregates, to confirm their anti-PD potential. Moreover, the neuroprotective activity of these compounds was also verified in a *C. elegans* assay, a well-validated PD animal model, by observing the neurodegeneration of the cephalic (CEP) neurons. Finally, the ability to cross the blood-brain barrier (BBB), an essential feature for achieving a CNS effect, was preliminarily investigated for all the hybrids by means of an *in vitro* parallel artificial membrane permeability (PAMPA)-BBB assay.

Moreover, to gain insight on one of the possible underlying mechanisms of action, the GSK-3 α/β (Ser21/9) kinase activity was assessed for the most potent and interesting derivative 5 (see Figure S1, Supporting Information).

GSK-3 β Inhibition. A luminescence method was employed to assess the GSK-3 β inhibitory effect of the synthesized compounds by using a human recombinant enzyme.²⁸ The compounds 4–7 were first tested at the highest 10 μ M concentration, then, for derivatives showing an inhibition percentage over 50%, the IC₅₀ value was determined by performing a linear regression analysis and using 4-benzyl-2-methyl-1,2,4-thiadiazolidine-3,5-dione as the reference compound.²⁹ While 4 and 7 when tested at 10 μ M concentration showed a low GSK-3 β inhibitory effect (40% and 46%, respectively), for 5 and 6 low micromolar IC₅₀ values of 8.4

Table 1. Inhibition of GSK-3 β Enzymatic Activity by the Curcumin-Fumarate Hybrids (4–7)

Compd				GSK-3 β inhibition	
	R	R ¹	R ²	IC ₅₀ (μ M) ^a \pm SEM	inhibition (%) ^{a,b}
4	OCH ₃	OCH ₃	OCH ₂ CH ₃	>10	40 %
5	OBn	OCH ₃	OCH ₂ CH ₃	8.39 \pm 0.34	
6	OBn	OBn	OCH ₂ CH ₃	6.09 \pm 0.53	
7	OBn	OBn	OH	>10	46 %

^aValues are mean \pm SD of two independent measurements, each performed in triplicate. SEM = standard error of the mean. ^bInhibition % of GSK-3 β activity at the concentration of 10 μ M of the tested compounds.

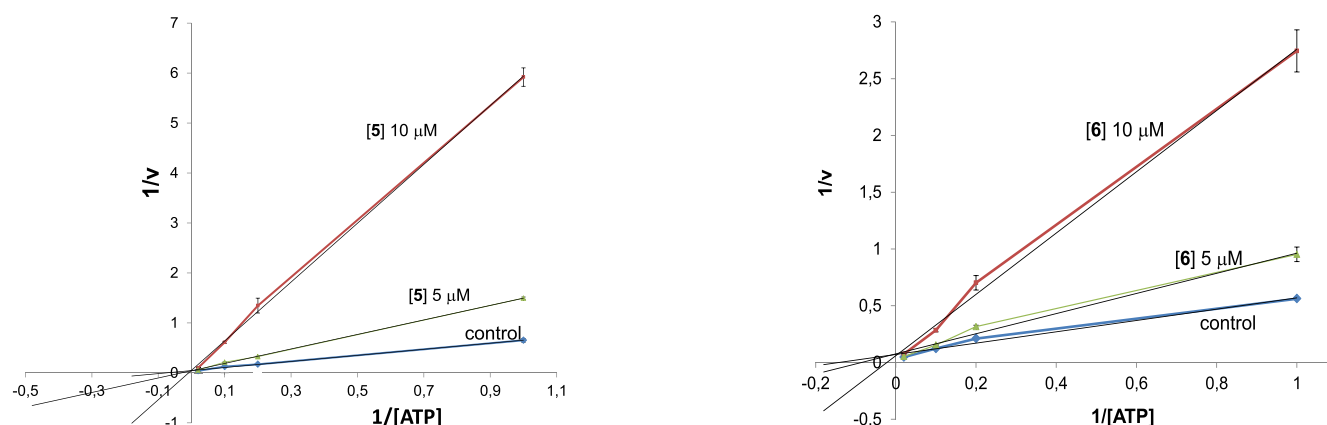


Figure 2. Kinetic data for the curcumin-DEF hybrids 5 and 6. In the reaction mixture, the concentration of compounds employed is reported in the plot, the concentration of the substrate is constant (25 μ M), and the concentration of ATP changes from 1 to 50 μ M. Each point is the mean of two different experiments analyzed in triplicate.

and 6.1 μ M, respectively, were recorded (Table 1). This result could be exciting, since a smooth therapeutic inhibition of GSK-3 β , allowing for CNS upregulated enzyme levels to return to physiological levels while not affecting normal peripheral enzyme levels, has been indicated as a safe approach.³⁰ Thus, the mechanism of inhibition as regards competition with ATP was investigated for 5 and 6. A kinetic study was performed in which the concentrations of both ATP and tested compounds were varied, while the concentration of the substrate was kept constant. By observing the graphs (Figure 2) reporting the double reciprocal plot of the data, we can speculate that 5 and 6 act as noncompetitive inhibitors of ATP binding, as by increasing concentration of ATP from 1 to 50 μ M, enzymatic inhibition is not affected.

Cytotoxicity. The 3-(4,5-dimethylthiazol-2-yl)-2,5-diphenyltetrazolium bromide (MTT) assay was used to evaluate the cytotoxic effects of the compounds. The SH-SY5Y cells were exposed to compound concentrations ranging from 1.25 to 40 μ M for 24 h, and cell viability was evaluated by MTT. The treatment of SH-SY5Y cells with all the tested compounds at the concentrations lower than 10 μ M did not affect cell viability (see Figure S9, Supporting Information). Thereby, the

concentration of 5 μ M was selected to perform all the following assays in SH-SY5Y.

Antioxidant Activity. Oxidative stress represents a remarkable pathological feature in NDDs; it is the consequence of an imbalance between the formation of reactive radical species, among others ROS, and the function of many defense antioxidant enzymes. Initially, the potential of compounds 4–7 as indirect antioxidants was investigated³¹ by assessing their capability to protect from oxidative stress through prevention of ROS formation upon exposure to *tert*-butyl hydroperoxide (*t*-BuOOH). In detail, SH-SY5Y cells were first chronically treated for 24 h (the time necessary to activate the endogenous antioxidant system) with 4–7 (5 μ M) and then exposed to 100 μ M of *t*-BuOOH for 30 min; DMF (5 and 10 μ M) was employed as the reference compound. Then, the intracellular ROS formation was detected by fluorescent probe 2',7'-dichlorodihydrofluorescein diacetate (H₂DCF-DA). The results, depicted in Figure 3, show a significant reduction in *t*-BuOOH-induced intracellular ROS formation after the treatment with compounds 4 and 5 and DMF but not with 6 and 7.

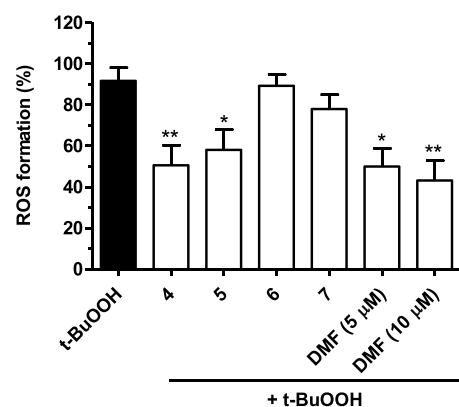


Figure 3. Antioxidant activity of compounds 4–7 and DMF against *t*-BuOOH-induced ROS formation in SH-SY5Y cells. Cells were treated with compounds 4–7 (5 μM) and DMF (5 and 10 μM) for 24 h and then with *t*-BuOOH (100 μM) for 30 min. At the end of treatment, the ROS formation was evaluated by probe H₂DCF-DA. Results are expressed as mean ± SEM of at least three independent experiments (**p* < 0.05 and ***p* < 0.01 vs cells treated with *t*-BuOOH at one-way ANOVA with the Dunnett post hoc test).

By observing the reduction of ROS levels following a long treatment of the curcumin-DEF hybrids before the treatment with *t*-BuOOH, we hypothesized that the antioxidant effect might likely result from an increase in levels of GSH. This endogenous antioxidant plays critical roles in protecting cells against oxidative stress damage.³² Thus, the intracellular GSH levels were analyzed by employing the same experimental conditions used to evaluate the indirect antioxidant effect by fluorescent probe monochlorobimane (MCB). Treatment of SH-SY5Y cells with 5 μM of compounds 4–7 determined an increase in intracellular GSH levels (Figure 4A). The most active compounds were 4 and 5, with a 4-fold increase in GSH levels as compared to control. These effects were significantly higher than those elicited by DMF, a well-known inducer of GSH biosynthesis for which 2–3-fold increases were observed when tested at concentrations of 5 and 10 μM (Figure 4A). For the most promising compounds 4 and 5, the effect on GSH levels at different times (3–24 h) was studied. Figure 4B shows a significant increase of GSH quantity after 12 and 24 h of treatment, suggesting that the effects of these compounds could likely be ascribed to their ability to activate the transcription of GSH.

Activation of the Nrf2/ARE Pathway. An impairment of the transcriptional activity of Nrf2, the master regulator of neuronal adaptation to an oxidant environment, could be a consequence of an aberrant activity of the enzyme GSK-3β, which, in turn, is induced by pathological conditions including oxidative stress and disrupted redox balance. These events trigger a feed-forward loop, a distinct feature of neurodegenerative disorders, determining a decrease in cytoprotective effects against cellular insults. Recent studies indicate that GSK-3β, as a negative regulator of Nrf2, participates in the distribution of Nrf2 inside and outside the nucleus.⁷ In particular, the activation of GSK-3β leads to Nrf2 nuclear export and degradation at the cytosolic level.

In light of these findings, 4 and 5 emerged as the most promising to be further studied regarding their effect on the Nrf2/ARE pathway. First, the nuclear-cytoplasmic Nrf2 shuttling cycle was studied in SH-SY5Y cells, and by observing the Western blotting, both tested compounds at 5 μM were

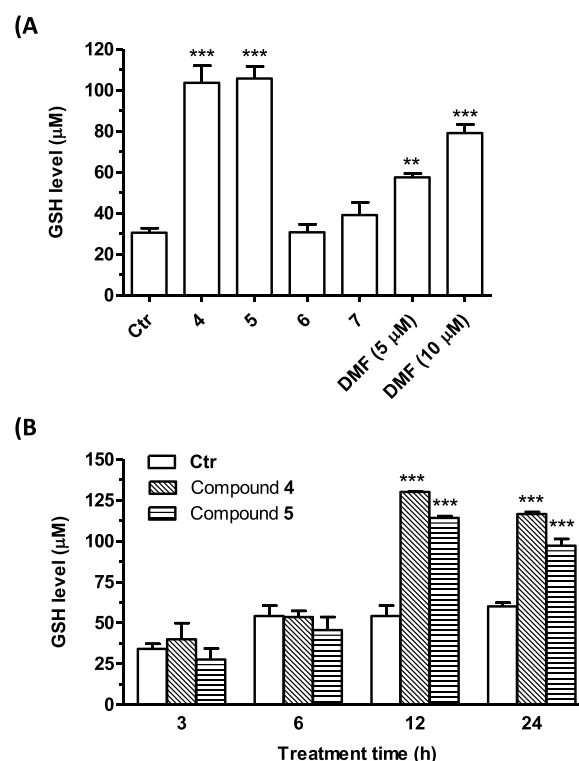


Figure 4. Effects of compounds 4–7 and DMF on GSH levels in SH-SY5Y cells. Cells were treated with (A) compounds 4–7 (5 μM) and DMF (5 and 10 μM) for 24 h. (B) Cells were treated with compounds 4 and 5 (5 μM) for different times (3, 6, 12, and 24 h). At the end of the treatment, the GSH levels were evaluated by probe MCB. Results are expressed as mean ± SEM of at least three independent experiments (***p* < 0.01 and ****p* < 0.001 vs untreated cells at one-way ANOVA with the Dunnett post hoc test).

seen to induce the nuclear translocation of Nrf2 both after short-term (1 and 3 h) and long-term treatments (6 h). The maximum ratio between nuclear and cytosolic Nrf2 levels was detected after a 3 h treatment for both compounds, while a slight reduction was observed after 6 h. These data suggested that compounds 4 and 5 induced a partial cytosolic redistribution of Nrf2 without altering its clearance (Figure 5A). Moreover, these results suggested a sustained Nrf2 activation together with a binding to the ARE sequence by the tested compounds. The activation and nuclear translocation of Nrf2 by 4 and 5 were also supported by an observed increase in Nrf2/ARE binding activity (Figure 5B). Briefly, these analogues showed superior effects to DMF, when tested at 5 μM.

To further confirm the increase in Nrf2 transcriptional activity upon treatment with 4 and 5, the mRNA levels of NQO1, a Nrf2 target gene, were evaluated in SH-SY5Y cells (Figure 5C). In the experimental conditions, 5 μM of the tested compounds showed a significant ability to increase NQO1 mRNA levels in SH-SY5Y cells after 12 and 24 h of treatment.

Neuroprotective Profile. The neuroprotective effects of curcumin-DEF hybrids 4 and 5 were investigated in some well-characterized *in vitro* models of AD and PD to gain insight into their therapeutic potential. In detail, the ability of the selected compounds to prevent SH-SY5Y cell death, induced by Aβ_{1–42} oligomers and 6-OHDA, was examined.

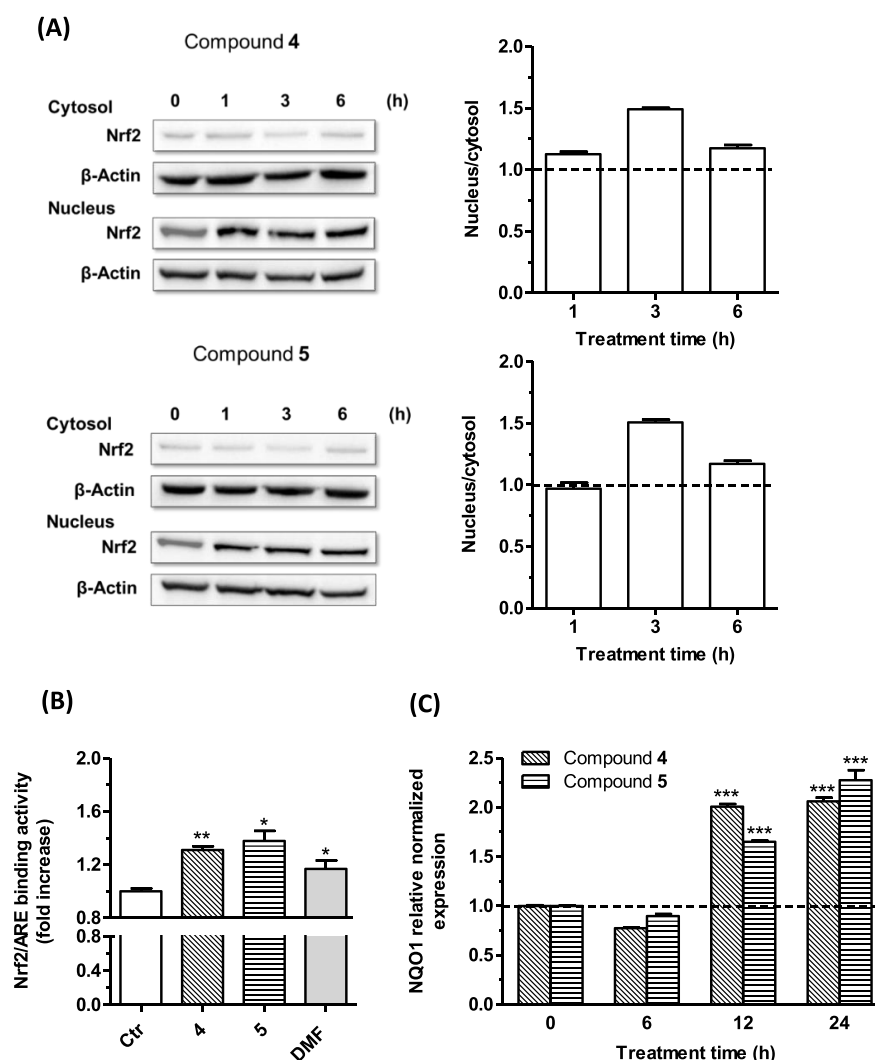


Figure 5. Effects of compounds 4 and 5 on the Nrf2/ARE signaling pathway (A and B) and NQO1 gene expression (C) in SH-SY5Y cells. (A) Cells were treated with compounds 4 and 5 (5 μ M) for different times (1, 3, and 6 h). Translocation of Nrf2 from the cytosol to the nucleus was evaluated by Western blotting. Data are expressed as a ratio between nuclear Nrf2 and cytoplasmic Nrf2 levels and reported as mean \pm SEM of at least three independent experiments. (B) Cells were treated with compounds 4 and 5 (5 μ M) and DMF (5 μ M) for 6 h. The Nrf2/ARE binding activity was determined by an ELISA assay. Results are expressed as fold increase versus untreated cells and reported as mean \pm SEM of at least three independent experiments (** p < 0.01 and * p < 0.05 versus untreated cells at the t -test). (C) Cells were treated with compounds 4 and 5 (5 μ M) for different times (6, 12, and 24 h). The NQO1 expression was determined by RT-PCR. Results are expressed as the relative normalized expression and reported as mean \pm SEM of at least three independent experiments (*** p < 0.001 versus untreated cells at one-way ANOVA with the Dunnett post hoc test).

In Vitro Model of AD. Intracellular accumulation of soluble $A\beta_{1-42}$ oligomers is responsible for neurotoxic effects, such as neuronal death, and represents a key event in AD pathogenesis.³³ Based on the promising data obtained, the most active compounds 4 and 5 were selected to be studied by using neurotoxic $A\beta_{1-42}$ oligomers—based on an *in vitro* model of AD. Briefly, SH-SY5Y cells were incubated with 5 μ M concentration of the selected analogues for 24 h, followed by $OA\beta_{1-42}$ oligomers treatment (10 μ M) for 4 h (Figure 6A). Both tested compounds failed to prevent $A\beta_{1-42}$ oligomers-induced cell death, indicative of their incapability to serve as $A\beta$ -based therapeutics.

In Vitro Model of PD. The neurotoxin 6-OHDA provides an *in vitro* lesion model by inducing CNS oxidative damage and neuroinflammation suitable for assessing the neuroprotective potential of PD therapeutics.³⁴ Consistent with

these effects, 6-OHDA (100 μ M, for 2 h) was employed to induce damage in SH-SY5Y cells previously treated with 4 and 5 (5 μ M, for 24 h). The results, depicted in Figure 6B, show that both the compounds mitigate the 6-OHDA-induced decrease in cell viability; this specific effect underlines potential usefulness of the tested analogues in the PD therapeutic area.

Assessment of the α -syn aggregate formation was performed to corroborate the above results. TagGFP2- α -syn SH-SY5Y cells were treated for 24 h with 5 μ M of 4 and 5 and then with 100 μ M of 6-OHDA. After a 2 h incubation, the presence of α -syn aggregates was visualized by fluorescence microscopy analysis and quantified (Figure 7). Both tested compounds were seen to significantly decrease the levels of toxic α -syn aggregates elicited by 6-OHDA.

Neuroprotective Effects in an *C. elegans* Model of PD. The nematode *Caenorhabditis elegans* (*C. elegans*) has been

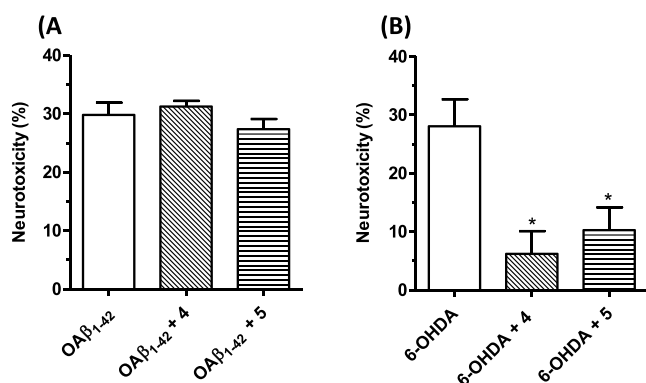


Figure 6. Effects of 4 and 5 on neurotoxicity induced by OAβ₁₋₄₂ oligomers and 6-OHDA in SH-SY5Y cells. (A) Cells were incubated with 4 and 5 (5 μM, for 24 h) and then treated with OAβ₁₋₄₂ (10 μM, for 4 h). (B) Cells were incubated with compounds 4 and 5 (5 μM, for 24 h), then treated with 6-OHDA (100 μM, for 2 h), and then starved in complete medium for 22 h. The neurotoxicity was evaluated by an MTT assay. Data are expressed as percentages of neurotoxicity versus cells treated with Aβ₁₋₄₂ oligomers or 6-OHDA and reported as mean ± SEM of at least three independent experiments (* *p* < 0.05 versus cells treated with 6-OHDA at one-way ANOVA with the Dunnett post hoc test).

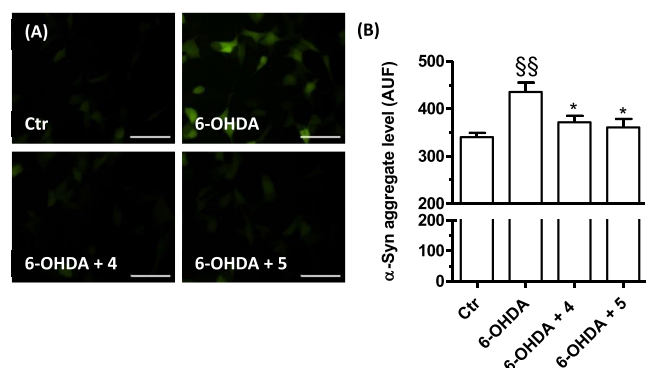


Figure 7. Effects of compounds 4 and 5 on α-syn aggregates induced by 6-OHDA in TagGFP2-α-syn SH-SY5Y cells. Cells were treated with compounds 4 and 5 (5 μM, for 24 h) and then with 6-OHDA (100 μM, for 2 h). At the end of incubation, the α-syn aggregates level was detected by fluorescence microscope. (A) Representative images of α-syn aggregates. (B) Quantification of the α-syn aggregates level. Data are expressed as mean fluorescence intensity ± SEM of at least three independent experiments (§§ *p* < 0.01 vs untreated cells, * *p* < 0.05 vs cells treated with 6-OHDA at one-way ANOVA with the Bonferroni post hoc test). Scale bars: 50 μm.

increasingly employed as a genetically tractable *in vivo* model to study the molecular mechanisms involved in several NDDs due to a short life cycle, fast reproduction, and a highly conserved inheritance (genetic basis).³⁵ This invertebrate model offers the opportunity to take advantage of the significant conservation of genes and metabolic pathways common to both invertebrates and humans. At the neuronal level, the adult wild-type *C. elegans* organism contains only eight DA neurons that repeat the features of DA neurons of mammalian, making it possible to simplify the investigations considerably. In the transgenic BY250 [*vtIs7* (*Pdat-1::GFP*)] strain, six DA neurons in the head, namely the four sensory cephalic (CEP) and the two anterior deirid (ADE) neurons, express the green fluorescent protein (GFP) and can be clearly visualized by fluorescence microscopy analysis and thus scored

over time.³⁶ Indeed, in this model, investigations of DA neurons degeneration *in vivo* are feasible through a first exposition of the nematode to PD-inducing toxin, namely 6-OHDA, followed by direct visualization of the GFP-labeled DA neurons.³⁷ It is thus possible to screen small molecules for their anti-PD potential, in terms of rescue of the DA neurodegeneration phenotype manifested upon neurotoxin exposure, through visualization and scoring of the alterations of CEP neuron count or neuronal morphology. Interestingly, it has been previously demonstrated that in *C. elegans*, GSK-3, the orthologue of mammalian GSK-3α/β, prevents SKN-1 (orthologue of mammalian Nrf2) accumulation in the nuclei and constitutive induction of antioxidant gene expression in the intestine. This effect makes it possible the identification of neuroprotective agents with the ability to activate Nrf2 through the inhibition of GSK-3.³⁸ The curcumin-DEF hybrids 4 and 5 were investigated in the above *C. elegans* model for their protective effects on 6-OHDA-induced degeneration of a subclass of DA neurons. Animals were incubated with 5 μM concentration of 4 and 5, in the presence of 5 mM of 6-OHDA, for 30 min. After 72 h, the animals were studied by examining the four CEP neurons. Degenerating CEP neurons were morphologically analyzed and quantified (Figure 8). We recorded that in animals treated with 6-OHDA, 68% of CEP neurons degenerated. In contrast, cotreatment with 5 caused a partial rescue of this phenotype, with a decreased degeneration percentage (55%) of CEP neurons (Figure 8D). Otherwise, 4 cotreatment displayed no rescue of the phenotype (67% of neurons degenerating, Figure 8D). The visual study of DA neuronal cell bodies and neurites (Figures 8A–C) showed that in wild type untreated animals all CEP neurons are visible and show a normal morphology (Figure 8A), in animals treated with 6-OHDA dendrites and cell bodies degenerated (Figure 8B). The cotreatment with compound 5 prevented the degeneration of some of the CEP dendrites, and some CEP cell bodies were still visible, confirming a partial rescue of the 6-OHDA-induced toxic effects. From these results, it emerged that analogue 5, but not 4, can protect neurons from PD-inducing toxin insult *in vivo*.

Concerning the mechanisms that activate Nrf2 after treatment with the compounds 4 and 5, our results suggest that part of the neuroprotective effects is Keap1-dependent. It is plausible that Nrf2 is released from Keap1 upon redox modifications and adduct formation with the molecules. However, other pathways, such as the activation of PI3K/AKT and subsequent inhibition of GSK-3β, a negative regulator of Nrf2, can also activate Nrf2. In this regard, under chronic oxidative stress observed in NDDs, the activation of GSK-3β can become predominant with an increase of the cytoplasmic degradation of Nrf2. Among the tested compounds, only 5 effectively inhibited GSK-3β activity, also showing neuroprotective effects in a transgenic *C. elegans* model of PD, where the activation of GSK-3β is closely involved in Nrf2 regulation as well as oxidative stress defense.³⁵ The ability of the most potent compound 5 in a *C. elegans* model of PD to inhibit the GSK-3β kinase activation, in terms of inactive phospho-GSK-3α/β (Ser21/9) increase, was also evaluated in SH-SY5Y cells. After 1 h of incubation, compound 5 was seen to increase phospho-GSK-3α/β (Ser21/9) levels, suggesting the ability of this new derivative to inhibit the activation of GSK-3α/β also in neuronal cells (see Figure S1, Supporting Information).

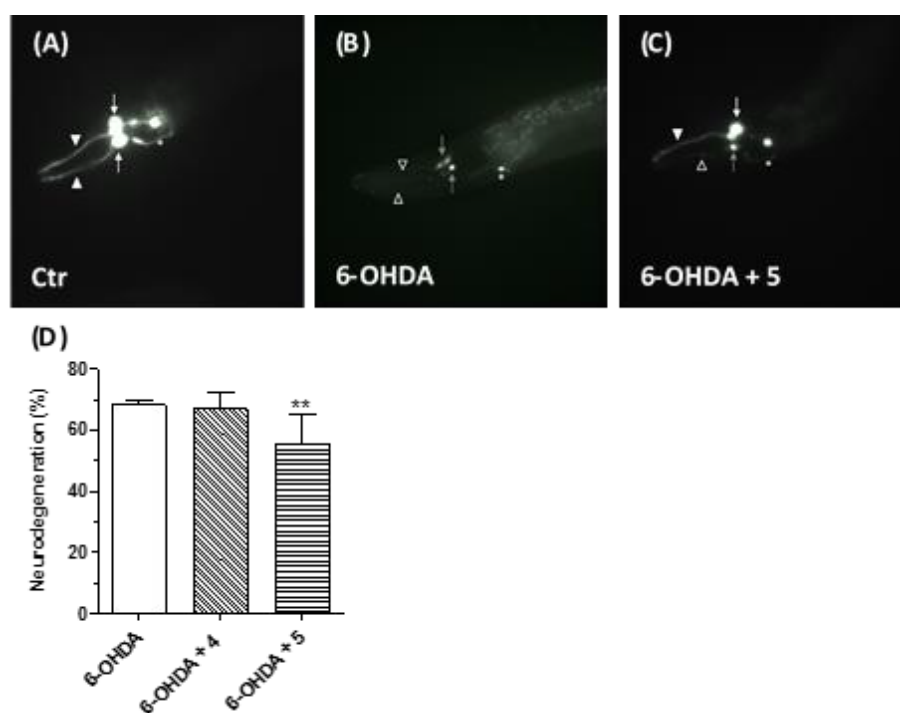


Figure 8. Effects of 4 and 5 on 6-OHDA-induced neurodegeneration in *C. elegans*. Animals were treated with 4 or 5 (5 μ M) in the presence of 6-OHDA (5 mM) for 30 min. At the end of incubation, treated animals were placed on fresh agar plates for 72 h and then visualized as described in the [Materials and Methods](#) section. (A) In nontreated *vtIs7* [*pdat-1::GFP*] transgenic animals, dopaminergic neurons express GFP, with two of the four CEP cell bodies (white arrows) and relative dendrites (arrowheads) visible in this focal plane in the head. (B) 6-OHDA treatment causes the degeneration of CEP dendrites (empty arrowheads) and two cell bodies (gray arrows), in treated animals. The other two CEP neurons are not visible anymore. (C) Compound 5 cotreatment partially rescues the 6-OHDA-induced toxic effects, with degeneration of one of the CEP dendrites (empty arrowhead) but not the other (arrowhead) and with one CEP cell body still viable (white arrow) and one dying (gray arrow) in this focal plane. Pictures have been taken with epifluorescence microscopy; in all panels, the anterior part of the animal is on the left and ventral down. ADE neurons, which are less affected by 6-OHDA treatment, are also visible but were not scored (asterisks). (D) Quantification of degenerating CEP neurons. Data are expressed as percentages of degenerating neurons and reported as mean \pm SEM of at least three independent experiments. The number of animals observed is $n = 270, 130$, and 272 , respectively (** $p < 0.01$ versus animals treated with 6-OHDA at one-way ANOVA with the Kruskal–Wallis post hoc test).

Blood-Brain Barrier (BBB) Permeation. The BBB permeation represents an essential requirement for neurotherapeutic agents as it controls the capability of the drug to reach the CNS compartment at therapeutic concentrations. Thus, yet at an early drug discovery phase, the BBB permeability behavior of potential neurotherapeutics should be taken into account. This barrier is a compact boundary that manages exchanges between the CNS and the blood compartments.³⁹ A parallel artificial membrane permeability assay (PAMPA) is a high-throughput technique developed to simulate the transcellular passive diffusion mechanism by which drugs reach the CNS. Thus, the capacity of all the newly synthesized curcumin-fumarate hybrids to enter the CNS was preliminarily explored using a PAMPA-BBB methodology employing a brain lipid porcine membrane.⁴⁰ The *in vitro* permeability (Pe) of compounds 4–7 (Table 2) together with 10 commercial drugs (see Table S1, Supporting Information), through a lipid membrane extract, was determined. A good correlation between experimental-described values was obtained (see Figure S8, Supporting Information). Taking into account guidelines established in the literature for the prediction of BBB permeation, compounds showing a Pe value superior to $2.26 \times 10^{-6} \text{ cm s}^{-1}$ could be regarded as able to permeate the brain compartment and thus classified as (CNS+).⁴¹ Based on these premises, in light of the obtained results, all the synthesized curcumin-DEF hybrids (4–6) proved to be able

Table 2. Permeability ($Pe \text{ } 10^{-6} \text{ cm s}^{-1}$) in the PAMPA-BBB Assay for Compounds 4–7 with Their Predictive Penetration in the CNS^a

compound	$Pe \text{ } (10^{-6} \text{ cm s}^{-1})^b$	prediction
4	2.5 ± 0.3	CNS +
5	4.8 ± 0.4	CNS +
6	4.5 ± 0.6	CNS +
7	1.7 ± 0.1	CNS +/CNS –

^aThe PBS:EtOH (70:30) mixture was used as solvent. ^bData are the mean \pm SD of two independent experiments.

to cross the BBB by passive permeation, while curcumin-fumaric acid (7) presented a borderline profile (CNS \pm).

Chemical Stability Study. Conscious of the liabilities that might affect the newly synthesized curcumin-fumarate hybrids involving both the curcumin scaffold and the ester function, the chemical stability of the ester-based 6 and its carboxylic-acid counterpart 7 was studied by RP-HPLC.^{21b} In detail, by following a previously reported methodology, in the working conditions, compound 6 proved to be stable, while for derivative 7 the formation of a degradation product was observed (see Figure S10, Supporting Information).

CONCLUSIONS

The significant therapeutic potential of multitarget agents for contrasting the multifactorial nature of NDDs prompted us to rationally design a new series of dual GSK-3 β inhibitors/Nrf2 inducers. In detail, a rational design strategy was performed, by which previously discovered curcumin-based GSK-3 β inhibitors (1–3) were joined to a fragment of a Nrf2 modulator, namely DEF. The obtained small series of curcumin-DEF hybrids (4–7) was tested against the selected targets GSK-3 β and Nrf2, correlated to inflammation and oxidative stress, the well-recognized NDDs copathogenic factors. Regarding GSK-3 β inhibition, derivatives 5 and 6 turned out to be the most effective of the series, showing low-micromolar potencies. In parallel, analogues 4 and 5 increased GSH intracellular levels through the activation of the Nrf2/ARE pathway, with particular reference to the capability to induce Nrf2 nuclear translocation and intensify Nrf2/ARE binding activity. These last derivatives emerged as dual GSK-3 β /Nrf2 modulators and, due to their good BBB-penetrating capabilities, could be regarded as lead compounds, worth investigating for their neuroprotective potential. In detail, 4 and 5 demonstrated a protective effect against the neurotoxicity induced by 6-OHDA, which proved to be ineffective in protecting from A β _{1–42} oligomers insult. When studied in a transgenic *C. elegans* model of PD, compound 5 recorded a remarkable neuroprotective effect as, by observing transgenic *C. elegans* CEP dendrites and CEP cell bodies, its cotreatment provided a partial rescue of the toxic effects induced by 6-OHDA. Taken together, these data indicate derivative 5 as a very good lead compound for the development of PD therapeutics. Moreover, this molecule, due to its multipotent profile, could represent a lead compound worthy of further development to obtain disease-modifying PD therapeutics. In summary, this study corroborates the pivotal role of curcumin to serve as starting backbone for the design of multipotent therapeutics for NDDs cure.

MATERIALS AND METHODS

Chemistry. General Procedures. Chemical reagents and solvents were employed as commercial products with a high-grade purity. Melting points were determined in open glass capillaries, using a Büchi apparatus, and are uncorrected. Reaction courses were monitored by thin-layer chromatography (TLC) performed on precoated TLC plates (Merck Silica Gel 60 F254, layer 0.20 mm) and then visualized under a UV lamp (λ = 254 and 365 nm). Flash column chromatography (FCC) separations were performed on silica gel (Kieselgel 40, particle size 0.040–0.063 mm, Merck). ¹H NMR and ¹³C NMR spectra were recorded on a Varian INOVA spectrometer operating at 400 MHz; chemical shifts are reported as parts per million (ppm δ value). Standard abbreviations indicating spin multiplicities are given as follows: s (singlet), d (doublet), dd (doublet of doublet), t (triplet), br (broad), q (quartet), or m (multiplet). ESI-MS mass spectra were recorded on a Waters ZQ 4000 apparatus. All tested compounds were found to have >95% purity, as determined by RP-HPLC analysis, performed on a chromatograph MD210 plus diode array detector equipped with a 20 μ L loop valve and a Pu 1580 pump (Jasco Europe, Italy) by using a Phenomenex Luna 5 μ m C18 column (150 \times 4.60 mm) as stationary phase, and a mixture of H₂O/ACN/ (50:50 v/v) for 4 and 6 and H₂O/ACN (40:60, v/v) for 5 and 7 as mobile phase; detection at λ = 280 and 425 nm, flow rate of 1.0 mL/min. Compound names are in accord with the naming algorithm developed by CambridgeSoft Corporation used in Chem-BioDraw Ultra 19.0. Compounds 1–3 have been synthesized as previously reported, and the spectroscopic data are in agreement with those reported in the literature.^{21b}

General Procedure for the Synthesis of Curcumin-DEF Hybrids (4–6). In a two neck flask equipped with a nitrogen inlet system and a rubber sept, NaH (60% dispersion in mineral oil, 1.5 molar equiv) was suspended in anhydrous THF (20.0 mL) and then dropwise added by a solution of 1–3 (1.00 mmol) in anhydrous THF (25.0 mL) at 0 °C; the obtained mixture was stirred for 30 min at 0 °C and then for 1 h at rt. Afterward, upon cooling to 0 °C, a solution of ethyl acetylenecarboxylate (2.0 molar equiv) in anhydrous THF (1.0 mL) was added *via* syringe, and the reaction was stirred at rt for 18 h. Then, the mixture was poured into ice/water (400 mL) followed by extraction with EtOAc (3 \times 50.0 mL). The organic phases were combined and concentrated to dryness to give a residue that was then subjected to an FCC purification, followed by crystallization from a suitable solvent to afford the desired compounds 4–6.

Ethyl (2E,4Z,6E)-5-Hydroxy-7-(4-methoxyphenyl)-4-((E)-3-(4-methoxyphenyl)acryloyl)hepta-2,4,6-trienoate (4). According to the general procedure, reaction of NaH (0.09 g, 2.25 mmol), 1 (0.50 g, 1.5 mmol), and ethyl acetylenecarboxylate (0.30 mL, 3.0 mmol) gave a crude product that underwent FCC separation by using a 9.5:0.5 mixture of PE/EtOAc as eluent, followed by crystallization from EtOH, to obtain a red solid; mp 122–124 °C, 71% yield. ¹H NMR (CDCl₃): δ 1.37 (t, 3H, *J* = 7.2 Hz, CH₃), 3.87 (s, 6H, OCH₃), 4.31 (q, 2H, *J* = 6.8 Hz, OCH₂), 5.96 (d, 1H, *J* = 15.6 Hz, =CH), 6.94 (d, 4H, *J* = 8.4 Hz, Ar), 7.00 (d, 2H, *J* = 15.6 Hz, =CH), 7.55 (d, 4H, *J* = 8.4 Hz, Ar), 7.79 (d, 2H, *J* = 15.2 Hz, =CH), 7.89 (d, 1H, *J* = 15.6 Hz, =CH) (see Figure S2, Supporting Information). ¹³C NMR (CDCl₃): δ 14.5, 55.6 (2C), 60.7, 110.1, 114.6 (4C), 118.7 (2C), 122.7, 128.0 (2C), 130.4 (4C), 139.1, 142.7 (2C), 161.8 (2C), 167.0, 183.9 (2C) (see Figure S3, Supporting Information). MS-ESI (*m/z*): 457 (M + Na).

Ethyl (2E,4Z,6E)-7-(4-(Benzyloxy)phenyl)-5-hydroxy-4-((E)-3-(4-methoxyphenyl)acryloyl)hepta-2,4,6-trienoate (5). According to the general procedure, reaction of NaH (0.09 g, 2.25 mmol), 2 (0.40 g, 1.00 mmol), and ethyl acetylenecarboxylate (0.30 mL, 3.0 mmol) gave a crude product that underwent FCC separation by using a 9.5:0.5 mixture of PE/EtOAc as eluent, followed by two sequential treatments with EtOAc/nE and EtOH. A dark red solid was obtained, mp 63–65 °C, 41% yield. ¹H NMR (CDCl₃): δ 1.35 (t, 3H, *J* = 7.2 Hz, CH₃), 3.87 (s, 3H, OCH₃), 4.31 (q, 2H, *J* = 6.8 Hz, OCH₂), 5.13 (s, 2H, Bn OCH₂), 5.96 (d, 1H, *J* = 15.6 Hz, =CH), 6.94 (d, 2H, *J* = 8.7 Hz, Ar), 7.00 (d, 2H, *J* = 15.2 Hz, =CH), 7.01 (d, 2H, *J* = 8.0 Hz, Ar), 7.32–7.47 (m, 5H, Bn Ar), 7.55 (d, 4H, *J* = 7.6 Hz, 4CH, Ar), 7.78 (d, 2H, *J* = 15.6 Hz, CH=CH), 7.89 (d, 1H, *J* = 15.6 Hz, CH=CH) (see Figure S4, Supporting Information). ¹³C NMR (CDCl₃, 101 MHz): δ 14.5, 55.6, 60.7, 70.3, 110.1, 114.6 (2C), 115.5 (2C), 118.7, 118.9, 122.7, 127.6 (2C), 127.9, 128.2, 128.3, 128.8 (2C), 130.4 (4C), 136.5, 139.1, 142.6, 142.7, 161.0, 161.8, 167.0, 183.8 (2C) (see Figure S5, Supporting Information). MS-ESI (*m/z*): 533 (M + Na).

Ethyl (2E,4Z,6E)-7-(4-(Benzyloxy)phenyl)-4-((E)-3-(4-(benzyloxy)phenyl)acryloyl)-5-hydroxyhepta-2,4,6-trienoate (6). According to the general procedure, reaction of NaH (0.09 g, 2.25 mmol), 3 (0.50 g, 1.00 mmol), and ethyl acetylenecarboxylate (0.30 mL, 3.0 mmol) gave a crude product that underwent FCC separation by using a 9.75:0.25 mixture of PE/acetone as eluent, followed by two sequential treatments with DCM/PE and EtOH. A yellow-brown solid was obtained, mp 153–155 °C, 84% yield. ¹H NMR (CDCl₃, 400 MHz): δ 1.38 (t, 3H, *J* = 7.2 Hz, CH₃), 4.31 (q, 2H, *J* = 6.8 Hz, OCH₂), 5.13 (s, 4H, Bn OCH₂), 5.95 (d, 1H, *J* = 15.6 Hz, =CH), 6.98 (d, 4H, *J* = 8.8 Hz, Ar), 6.99 (d, 2H, *J* = 15.4 Hz, =CH), 7.32–7.45 (m, 11H, OH and Bn Ar), 7.55 (d, 4H, *J* = 8.8 Hz, Ar), 7.78 (d, 2H, *J* = 15.2 Hz, =CH), 7.88 (d, 1H, *J* = 15.6 Hz, =CH) (see Figure S6, Supporting Information). ¹³C NMR (CDCl₃, 101 MHz): δ 14.5, 60.7, 70.3 (2C), 110.1, 115.5 (4C), 118.9 (2C), 122.7, 127.6 (4C), 128.2 (2C), 128.3 (2C), 128.8 (4C), 130.4 (4C), 136.5 (2C), 139.1, 142.6 (2C), 161.0 (2C), 167.0, 183.8 (2C) (see Figure S7, Supporting Information). MS-ESI (*m/z*): 609 (M + Na).

(2E,4Z,6E)-7-(4-(Benzyloxy)phenyl)-4-((E)-3-(4-(benzyloxy)phenyl)acryloyl)-5-hydroxyhepta-2,4,6-trienoic Acid (7). A KOH methanol solution (2.0 N, 0.62 mL) was added dropwise to a solution

of 6 (0.10 g, 0.17 mmol) in MeOH (4.4 mL) during a period of 30 min and under stirring; the obtained mixture was heated at 60 °C under stirring for 12 h. Then, the solvent was removed under reduced pressure to give a residue that was solubilized with Et₂O (30 mL) and then extracted with H₂O (3 × 30 mL). The aqueous phase was acidified with 37% HCl and then extracted with DCM (3 × 30 mL). The combined organic layers were washed with brine, dried over Na₂SO₄, filtered, and concentrated to dryness, affording a residue that was purified by two sequential treatments with DCM/PE and EtOH. A pale brown powder was obtained, mp 182–184 °C, 75% yield. ¹H NMR (acetone-*d*₆, 400 MHz): δ 5.19 (s, 4H, Bn OCH₂), 6.39 (d, 2H, *J* = 15.6 Hz, =CH), 7.08 (d, 4H, *J* = 8.8 Hz, Ar), 7.34–7.42 (m, 10H, Bn Ar), 7.49 (d, 4H, *J* = 7.6 Hz, Ar), 7.63 (d, 4H, *J* = 16.4 Hz, =CH), 7.63 (br, 1H, OH). ¹³C NMR (acetone-*d*₆, 101 MHz): δ 70.0 (2C), 110.1, 116.0 (4C), 119.0 (2C), 122.7, 127.6 (4C), 128.1 (2C), 128.3 (2C), 128.8 (4C), 130.5 (4C), 136.5 (2C), 139.0, 142.6 (2C), 160.9 (2C), 168.0, 183.9 (2C). ESI-MS-(*m/z*): 581 (*M* + Na).

GSK-3β Inhibition. The method of Baki et al. was followed for the inhibition of GSK-3β (see the Supporting Information for experimental details).²⁸

Kinetic Studies. Kinetic experiments were performed using the ADP-Glo Kinase Assay,⁴² in which ATP concentration varied from 1 to 50 μM, the concentrations of inhibitors employed were 5 and 10 μM, while the concentration of GS2 was kept constant (25 μM). Graphs (Figure 2) report the double reciprocal plot of the data.

Cell Cultures. Human neuronal SH-SY5Y cells (Sigma-Aldrich, St. Louis, MO, USA) and TagGFP2-α-synuclein SH-SY5Y cells (Innoprot, Bizkaia, Spain) were routinely grown in Dulbecco's modified Eagle's Medium supplemented with 10% fetal bovine serum, 2 mM L-glutamine, 50 U/mL penicillin, and 50 μg/mL streptomycin at 37 °C in a humidified incubator with 5% CO₂.

Intracellular ROS Formation. SH-SY5Y cells were seeded in a 96-well plate at 2 × 10⁴ cells/well, incubated for 24 h, and then treated with 5 μM concentration of compounds 4–7 and 5–10 μM concentrations of DMF at 37 °C for 24 h, in 5% CO₂. ROS formation was evaluated by using the fluorescent probe H₂DCF-DA, as previously described.⁴³

Measurement of Intracellular GSH. SH-SY5Y cells were seeded in a black 96-well plate at 2 × 10⁴ cells/well, incubated for 24 h, and then treated with compounds 4–7 (5 μM) and DMF (5–10 μM) for 24 h at 37 °C in 5% CO₂. In parallel, SH-SY5Y cells were seeded in 60 mm dishes at 2 × 10⁶ cells/dish, incubated for 24 h, and then treated with curcumin-DEF hybrids 4 and 5 (5 μM) for 3, 6, 12, and 24 h at 37 °C in 5% CO₂. GSH levels were evaluated by using the fluorescent probe MCB, as previously described.⁴⁴

Detection of Nrf2 Nuclear Translocation by Western Blotting. SH-SY5Y cells were seeded in 60 mm dishes at 2 × 10⁶ cells/dish, incubated for 24 h, and then treated with compounds 4 and 5 (5 μM) for 1, 3, and 6 h at 37 °C in 5% CO₂. At the end of treatment, cytosolic and nuclear extractions for Nrf2 nuclear translocation were performed by using a Nuclear Extract Kit (Active Motif, Carlsbad, CA, USA), according to the manufacturer's guidelines. Cytosolic and nuclear extracts (50 μg per sample) were separated by SDS-polyacrylamide gels and transferred onto nitrocellulose membranes, which were probed with primary Nrf2 (1:1000; Santa Cruz Biotechnology, Dallas, TX, USA) and secondary antibodies. ECL reagents (Pierce) were utilized to detect targeted bands. The same membranes were stripped and reprobed with β-actin antibody (1:1000; Sigma-Aldrich). Western blot bands were analyzed by densitometry, using Quantity One software (Bio-Rad, Hercules, CA, USA). Results are expressed as a ratio between nuclear and cytoplasmic Nrf2 levels.

Determination of the Active Nrf2 Protein Level. The levels of active Nrf2 protein were determined on the nuclear extracts (10 μg, see above) by using the DNA-binding ELISA TransAM Nrf2 Kit (Active Motif), according to the manufacturer's guidelines. In detail, the kit comprises a primary antibody able to recognize an epitope on Nrf2 protein upon ARE binding. In the treated cells, the amount of active Nrf2 protein is expressed as a fold increase in comparison to the corresponding untreated cells.

RNA Extraction and Quantitative Real-Time PCR. SH-SY5Y cells were seeded in 100 mm dishes at 2.5 × 10⁶ cells/dish, incubated for 24 h, and then treated with compounds 4 and 5 (5 μM) for different times (6, 12, and 24 h) at 37 °C and in 5% CO₂. Afterward, a cell suspension was pelleted, and RNA was extracted by the PureLink RNA Mini Kit (Life Technologies, Carlsbad, CA, USA) according to the manufacturer's guidelines. A total of 1 μg of RNA were used to synthesize cDNA using the SuperScript VILO MasterMix (Invitrogen, Carlsbad, CA, USA). Quantitative Real-Time PCR was carried out using SYBR Select Master Mix (Invitrogen), and relative normalized expression was calculated by comparing the cycle threshold (Ct) of the target gene to that of the reference genes beta-2 microglobulin (B2M) and TATA-box binding protein (TBP, Life Technologies). All reactions had three technical replicates, and each condition had three biological replicates. Relative quantification was calculated according to the ΔΔCt method (2^{−ΔΔCt}) with untreated cells as control. Primer sequences used in this study are listed in Table S2.

Aβ_{1–42} Oligomers Preparation for the Determination of Neuroprotective Activity. Aβ_{1–42} peptide (AnaSpec, Fremont, CA, USA) was first dissolved in 1,1,1,3,3,3-hexafluoroisopropanol to 1 mg/mL, sonicated, incubated at rt for 24 h, and lyophilized to obtain an unaggregated Aβ_{1–42} peptide film that was solubilized with DMSO and stored at −20 °C until use. The aggregation of Aβ_{1–42} peptide into oligomers was performed as previously described.⁴⁵

Neuroprotective Activity toward Aβ_{1–42} Oligomers. SH-SY5Y cells were seeded in a 96-well plate at 3 × 10⁴ cells/well, incubated for 24 h, and treated with compounds 4 and 5 (5 μM) for 24 h. Then, cells were treated with Aβ_{1–42} oligomers for 4 h. The neuroprotective activity, in terms of an increase in intracellular MTT granules, was measured by an MTT assay, as previously described (see the Supporting Information for experimental details).⁴⁶

Neuroprotective Activity toward 6-Hydroxydopamine. SH-SY5Y cells were seeded in a 96-well plate at 3 × 10⁴ cells/well, incubated for 24 h, and subsequently treated with compounds 4 and 5 (5 μM) for 24 h. Then, cells were treated with 6-hydroxydopamine (6-OHDA, 100 μM) for 2 h and starved in complete medium for 22 h. The neuroprotective activity was measured by using the MTT assay as previously described.⁴⁷ Data are expressed as a percentage of neurotoxicity versus untreated cells.

Detection of α-Synuclein Aggregation. TagGFP2-α-synuclein SH-SY5Y cells were seeded in a 96-well plate at 2 × 10⁴ cells/well, incubated for 24 h, and subsequently treated with curcumin-DEF hybrids 4 and 5 (5 μM) for 24 h at 37 °C in 5% CO₂. Then, cells were treated with 6-OHDA (100 μM) for 2 h at 37 °C in 5% CO₂. At the end of incubation, the aggregation of α-synuclein was detected using an inverted fluorescent microscope (Eclipse Ti-E, Nikon Instruments Spa, Florence, Italy). The intensity of fluorescence was directly proportional to the aggregation of α-synuclein. Data are expressed as arbitrary units of fluorescence.

C. elegans Methods. Nematodes were grown and handled following standard procedures, under uncrowded conditions, at 20 °C, on nematode growth medium (NGM) agar plates seeded with *Escherichia coli* strain OP50.⁴⁸ The transgenic strain used in this work is BY250 *vtIs7[pdat-1::Green Fluorescent Protein (GFP)]*.³⁶ 6-OHDA toxicity against DA neurons was assessed as previously described.^{37a,49,37b} *vtIs7[pdat-1::GFP]* were synchronized, and L1 larval stage animals were washed off the plate and incubated with a solution of 1% DMSO (Sigma-Aldrich), 1 mM ascorbic acid (Sigma-Aldrich), and 5 mM 6-OHDA (Sigma-Aldrich) for 0.5 h in dark conditions and gentle agitation (as control, to exclude that any rescue was caused by the DMSO solvent and not by synthetic compounds) or with a solution of compounds 4 or 5 (5 μM) dissolved in 1% DMSO, 1 mM ascorbic acid, and 5 mM 6-OHDA. Treated animals were transferred onto plates (without removal of 6-OHDA and the compounds), incubated for 72 h, and then placed on a freshly prepared 4% agar pad, immobilized using 0.01% tetramisole hydrochloride (Sigma-Aldrich). Animals were visualized using Zeiss Axioskop, equipped with epifluorescence and images collected with a Leica DM6000B microscope equipped with epifluorescence and the digital camera Hamamatsu C11440. Only the four dopaminergic CEP neurons were

analyzed and scored as degenerated when we observed any of the following defects: blebbing, disappearance or breaking of the dendrites, and disappearance or rounding of the cell bodies. Results are expressed as a percentage of degenerating neurons.

Statistical Analysis. Results are shown as mean \pm standard error (SEM) of three independent experiments. Statistical analysis was performed using one-way ANOVA with the Dunnett or Bonferroni or Kruskal–Wallis post hoc test and Student's *t*-test, as appropriate. Differences were considered significant at $p < 0.05$. Analyses were performed using GraphPad PRISM software (version 5.0; GraphPad Software, La Jolla, CA, USA) on a Windows platform.

CNS Penetration. An *in vitro* parallel artificial membrane permeability assay (PAMPA)-blood-brain barrier (BBB) was employed. Prediction of the brain penetration was evaluated using a parallel artificial membrane permeability assay (PAMPA)⁴⁰ (see the [Supporting Information](#) for experimental details).

Chemical Stability Study. The tested derivatives **6** and **7** were dissolved in DMSO (0.50 mg/mL), and the pH of the solution was adjusted to 7.4 using 50 mM phosphate. The obtained solutions were then maintained at 70 °C (oven) for 24 h and analyzed by RP-HPLC under the conditions reported in the [General Procedures](#) section.

■ ASSOCIATED CONTENT

■ Supporting Information

The Supporting Information is available free of charge at <https://pubs.acs.org/doi/10.1021/acscchemneuro.0c00363>.

NMR spectra of compounds **4–6**; GSK-3 β activity of compound **5**; PAMPA-BBB assay: *Pe* values of 10 commercial drugs and linear correlation among experimental-reported *Pe*; cytotoxicity of compounds **4–7**, TDZD, and DMF in SH-SY5Y cells; primer sequences for quantitative real-time PCR; RP-HPLC chromatograms (compounds **6** and **7**); and Materials and Methods (PDF)

■ AUTHOR INFORMATION

Corresponding Authors

Federica Belluti – Department of Pharmacy and Biotechnology, Alma Mater Studiorum - University of Bologna, 40126 Bologna, Italy; orcid.org/0000-0002-6365-5579; Email: federica.belluti@unibo.it

Andrea Tarozzi – Department for Life Quality Studies, Alma Mater Studiorum - University of Bologna, 47921 Rimini, Italy; orcid.org/0000-0001-7983-8575; Email: andrea.tarozzi@unibo.it

Authors

Rita Maria Concetta Di Martino – Department of Pharmacy and Biotechnology, Alma Mater Studiorum - University of Bologna, 40126 Bologna, Italy

Letizia Pruccoli – Department for Life Quality Studies, Alma Mater Studiorum - University of Bologna, 47921 Rimini, Italy

Alessandra Bisi – Department of Pharmacy and Biotechnology, Alma Mater Studiorum - University of Bologna, 40126 Bologna, Italy; orcid.org/0000-0003-4662-4743

Silvia Gobbi – Department of Pharmacy and Biotechnology, Alma Mater Studiorum - University of Bologna, 40126 Bologna, Italy

Angela Rampa – Department of Pharmacy and Biotechnology, Alma Mater Studiorum - University of Bologna, 40126 Bologna, Italy; orcid.org/0000-0002-8028-8758

Ana Martínez – Centro de Investigaciones Biológicas, CSIC, 28040 Madrid, Spain; orcid.org/0000-0002-2707-8110

Concepción Pérez – Centro de Investigaciones Biológicas, CSIC, 28040 Madrid, Spain

Loreto Martínez-González – Centro de Investigaciones Biológicas, CSIC, 28040 Madrid, Spain

Maria Paglione – Department of Biology, Agriculture and Food Science, National Research Council (CNR), Institute of Biosciences and BioResources (IBBR), 80131 Naples, Italy

Elia Di Schiavi – Department of Biology, Agriculture and Food Science, National Research Council (CNR), Institute of Biosciences and BioResources (IBBR), 80131 Naples, Italy

Francesca Seghetti – Department of Pharmacy and Biotechnology, Alma Mater Studiorum - University of Bologna, 40126 Bologna, Italy; orcid.org/0000-0003-0478-7341

Complete contact information is available at:

<https://pubs.acs.org/doi/10.1021/acscchemneuro.0c00363>

Author Contributions

[†]R.M.C.D.M. and L.P. contributed equally to this work.

Author Contributions

F.B. and A.T. conceived the project, supervised all contributions, and finalized the draft manuscript. R.M.C.D.M. supervised synthesis and purification of curcumin analogues and drafted the manuscript. F.S. synthesized the tested analogues and performed NMR spectra and HPLC analysis. A.B., S.G., and A.R. assisted with the purification of the synthesized analogues and revision of the final version of the manuscript. L.P. carried out the experiments on cell viability, antioxidant activity, activation of the Nrf2/ARE pathway, and neuroprotective activity on neuroblastoma cells; prepared the figures; and drafted the text of the relative sections. A.M. supervised GSK-3 β and PAMPA assays. C.P. carried out the experiment on GSK-3 β . L.M.-G. carried out the PAMPA assay. E.D.S. conceived and supervised evaluation of neuroprotective effects in the *C. elegans* model of PD. M.P. performed studies on the *C. elegans* model of PD.

Notes

The authors declare no competing financial interest.

■ ACKNOWLEDGMENTS

This work was supported by the University of Bologna (RFO funds), MCIU (grant no. SAF2016-76693-R), and ISCIII CIBERNED (CB18/05/00040) and EDS, partially funded by the CNR project NUTR-AGE (FOE-2019, DSB.AD004.271). The authors thank M. Aschner (Albert Einstein College of Medicine, New York, USA) for the *vtIs7* strain and Giuseppina Zampi for technical support (WormBase).

■ ABBREVIATIONS

AD, Alzheimer's disease; A β , amyloid- β ; ADE, anterior deirid; ARE, antioxidant response element; BACE-1, β -site amyloid precursor protein cleaving enzyme; BBB, blood-brain barrier; CEP, cephalic; CNS, central nervous system; H₂DCF-DA, 2',7'-dichlorodihydrofluorescein diacetate; DEF, diethyl fumarate; DMF, dimethyl fumarate; MTT, 3-(4,5-dimethylthiazol-2-yl)-2,5-diphenyltetrazolium bromide; FCC, flash column chromatography; FAEs, fumaric acid esters; GSH, glutathione; GSK-3 β , glycogen synthase kinase-3 β ; GFP, green fluorescent protein; Keap1, Kelch-like ECH associated protein1; LBs, Lewy bodies; 6-OHDA, 6-hydroxydopamine; NQO1, NAD(P)H: quinone oxidoreductase 1; NDDs, neurodegenerative diseases; Nrf2, nuclear factor-erythroid related factor 2; NF-kB, nuclear factor-kB; MCB, monochlorobimane; PD, Parkinson's disease; p-tau, phospho-tau; ROS, reactive oxygen species; α -

syn, α -synuclein; *t*-BuOOH, *tert*-butyl hydroperoxide; TLC, thin-layer chromatography

REFERENCES

- (1) Carroll, W. M. (2019) The global burden of neurological disorders. *Lancet Neurol.* 18, 418–419.
- (2) Fu, H., Hardy, J., and Duff, K. E. (2018) Selective vulnerability in neurodegenerative diseases. *Nat. Neurosci.* 21, 1350–1358.
- (3) (a) Durrenberger, P. F., Fernando, F. S., Kashefi, S. N., Bonnert, T. P., Seilhean, D., Nait-Oumesmar, B., Schmitt, A., Gebicke-Haerter, P. J., Falkai, P., Grunblatt, E., Palkovits, M., Arzberger, T., Kretschmar, H., Dexter, D. T., and Reynolds, R. (2015) Common mechanisms in neurodegeneration and neuroinflammation: a BrainNet Europe gene expression microarray study. *J. Neural Transm. (Vienna)* 122, 1055–1068. (b) Gan, L., Cookson, M. R., Petrucelli, L., and La Spada, A. R. (2018) Converging pathways in neurodegeneration, from genetics to mechanisms. *Nat. Neurosci.* 21, 1300–1309.
- (4) Alam, P., Siddiqi, K., Chturvedi, S. K., and Khan, R. H. (2017) Protein aggregation: From background to inhibition strategies. *Int. J. Biol. Macromol.* 103, 208–219.
- (5) (a) Cheng, J., North, B. J., Zhang, T., Dai, X., Tao, K., Guo, J., and Wei, W. (2018) The emerging roles of protein homeostasis-governing pathways in Alzheimer's disease. *Aging Cell* 17, No. e12801. (b) Lehtonen, S., Sonninen, T. M., Wojciechowski, S., Goldsteins, G., and Koistinaho, J. (2019) Dysfunction of Cellular Proteostasis in Parkinson's Disease. *Front. Neurosci.* 13, 457.
- (6) (a) Fao, L., Mota, S. I., and Rego, A. C. (2019) Shaping the Nrf2-ARE-related pathways in Alzheimer's and Parkinson's diseases. *Ageing Res. Rev.* 54, 100942. (b) Kamat, P. K., Rai, S., Swarnkar, S., Shukla, R., and Nath, C. (2014) Mechanism of synapse redox stress in Okadaic acid (ICV) induced memory impairment: Role of NMDA receptor. *Neurochem. Int.* 76, 32–41.
- (7) Chen, X., Liu, Y., Zhu, J., Lei, S., Dong, Y., Li, L., Jiang, B., Tan, L., Wu, J., Yu, S., and Zhao, Y. (2016) GSK-3 β downregulates Nrf2 in cultured cortical neurons and in a rat model of cerebral ischemia-reperfusion. *Sci. Rep.* 6, 20196.
- (8) Ahmed, S. M., Luo, L., Namani, A., Wang, X. J., and Tang, X. (2017) Nrf2 signaling pathway: Pivotal roles in inflammation. *Biochim. Biophys. Acta, Mol. Basis Dis.* 1863, 585–597.
- (9) Ramsey, C. P., Glass, C. A., Montgomery, M. B., Lindl, K. A., Ritson, G. P., Chia, L. A., Hamilton, R. L., Chu, C. T., and Jordan-Sciutto, K. L. (2007) Expression of Nrf2 in neurodegenerative diseases. *J. Neuropathol. Exp. Neurol.* 66, 75–85.
- (10) Pajares, M., Cuadrado, A., and Rojo, A. I. (2017) Modulation of proteostasis by transcription factor NRF2 and impact in neurodegenerative diseases. *Redox Biol.* 11, 543–553.
- (11) Moreira, S., Fonseca, I., Nunes, M. J., Rosa, A., Lemos, L., Rodrigues, E., Carvalho, A. N., Outeiro, T. F., Rodrigues, C. M. P., Gama, M. J., and Castro-Caldas, M. (2017) Nrf2 activation by tauroursodeoxycholic acid in experimental models of Parkinson's disease. *Exp. Neurol.* 295, 77–87.
- (12) Liddell, J. R. (2017) Are Astrocytes the Predominant Cell Type for Activation of Nrf2 in Aging and Neurodegeneration? *Antioxidants* 6, 65.
- (13) Golpich, M., Amini, E., Hemmati, F., Ibrahim, N. M., Rahmani, B., Mohamed, Z., Raymond, A. A., Dargahi, L., Ghasemi, R., and Ahmadiani, A. (2015) Glycogen synthase kinase-3 β (GSK-3 β) signaling: Implications for Parkinson's disease. *Pharmacol. Res.* 97, 16–26.
- (14) Rojo, A. I., Sagarra, M. R., and Cuadrado, A. (2008) GSK-3 β down-regulates the transcription factor Nrf2 after oxidant damage: relevance to exposure of neuronal cells to oxidative stress. *J. Neurochem.* 105, 192–202.
- (15) Morphy, R., Kay, C., and Rankovic, Z. (2004) From magic bullets to designed multiple ligands. *Drug Discovery Today* 9, 641–651.
- (16) Uliassi, E., Piazzi, L., Belluti, F., Mazzanti, A., Kaiser, M., Brun, R., Moraes, C. B., Freitas, L. H., Gul, S., Kuzikov, M., Ellinger, B., Borsari, C., Costi, M. P., and Bolognesi, M. L. (2018) Development of a Focused Library of Triazole-Linked Privileged-Structure-Based Conjugates Leading to the Discovery of Novel Phenotypic Hits against Protozoan Parasitic Infections. *ChemMedChem* 13, 678–683.
- (17) Gameiro, I., Michalska, P., Tenti, G., Cores, A., Buendia, I., Rojo, A. I., Georgakopoulos, N. D., Hernandez-Guijo, J. M., Teresa Ramos, M., Wells, G., Lopez, M. G., Cuadrado, A., Menendez, J. C., and Leon, R. (2017) Discovery of the first dual GSK3 β inhibitor/Nrf2 inducer. A new multitarget therapeutic strategy for Alzheimer's disease. *Sci. Rep.* 7, 45701.
- (18) Bahadori, F., and Demiray, M. (2017) A Realistic View on "The Essential Medicinal Chemistry of Curcumin. *ACS Med. Chem. Lett.* 8, 893–896.
- (19) Di Martino, R. M., Luppi, B., Bisi, A., Gobbi, S., Rampa, A., Abruzzo, A., and Belluti, F. (2017) Recent progress on curcumin-based therapeutics: a patent review (2012–2016). Part I: Curcumin. *Expert Opin. Ther. Pat.* 27, 579–590.
- (20) (a) Tedesco, S., Zusso, M., Facci, L., Trenti, A., Boscaro, C., Belluti, F., Fadini, G. P., Skaper, S. D., Giusti, P., Bolego, C., and Cignarella, A. (2018) Bisdemethoxycurcumin and Its Cyclized Pyrrole Analogue Differentially Disrupt Lipopolysaccharide Signaling in Human Monocyte-Derived Macrophages. *Mediators Inflammation* 2018, 2868702. (b) Zusso, M., Mercanti, G., Belluti, F., Di Martino, R. M. C., Pagetta, A., Marinelli, C., Brun, P., Ragazzi, E., Lo, R., Stifani, S., Giusti, P., and Moro, S. (2017) Phenolic 1,3-diketones attenuate lipopolysaccharide-induced inflammatory response by an alternative magnesium-mediated mechanism. *Br. J. Pharmacol.* 174, 1090–1103.
- (21) (a) Bisceglia, F., Seghetti, F., Serra, M., Zusso, M., Gervasoni, S., Verga, L., Vistoli, G., Lanni, C., Catanzaro, M., De Lorenzi, E., and Belluti, F. (2019) Prenylated Curcumin Analogues as Multipotent Tools To Tackle Alzheimer's Disease. *ACS Chem. Neurosci.* 10, 1420–1433. (b) Di Martino, R. M., De Simone, A., Andrisano, V., Bisignano, P., Bisi, A., Gobbi, S., Rampa, A., Fato, R., Bergamini, C., Perez, D. I., Martinez, A., Bottegioni, G., Cavalli, A., and Belluti, F. (2016) Versatility of the Curcumin Scaffold: Discovery of Potent and Balanced Dual BACE-1 and GSK-3 β Inhibitors. *J. Med. Chem.* 59, 531–544. (c) Di Martino, R. M. C., Bisi, A., Rampa, A., Gobbi, S., and Belluti, F. (2017) Recent progress on curcumin-based therapeutics: a patent review (2012–2016). Part II: curcumin derivatives in cancer and neurodegeneration. *Expert Opin. Ther. Pat.* 27, 953–965.
- (22) Nelson, K. M., Dahlin, J. L., Bisson, J., Graham, J., Pauli, G. F., and Walters, M. A. (2017) The Essential Medicinal Chemistry of Curcumin. *J. Med. Chem.* 60, 1620–1637.
- (23) Bajorath, J. (2014) Activity artifacts in drug discovery and different facets of compound promiscuity. *FI000Research* 3, 233.
- (24) Jasial, S., Hu, Y., and Bajorath, J. (2017) How Frequently Are Pan-Assay Interference Compounds Active? Large-Scale Analysis of Screening Data Reveals Diverse Activity Profiles, Low Global Hit Frequency, and Many Consistently Inactive Compounds. *J. Med. Chem.* 60, 3879–3886.
- (25) de Freitas Silva, M., Pruccoli, L., Morroni, F., Sita, G., Seghetti, F., Viegas, C., and Tarozzi, A. (2018) The Keap1/Nrf2-ARE Pathway as a Pharmacological Target for Chalcones. *Molecules* 23, 1803.
- (26) Wilson, A. J., Kerns, J. K., Callahan, J. F., and Moody, C. J. (2013) Keap calm, and carry on covalently. *J. Med. Chem.* 56, 7463–7476.
- (27) This work constitutes part of the Ph.D. thesis of Dr. Rita M. C. Di Martino.
- (28) Baki, A., Bielik, A., Molnar, L., Szendrei, G., and Keseru, G. M. (2007) A high throughput luminescent assay for glycogen synthase kinase-3 β inhibitors. *Assay Drug Dev. Technol.* 5, 75–83.
- (29) Martinez, A., Alonso, M., Castro, A., Perez, C., and Moreno, F. J. (2002) First non-ATP competitive glycogen synthase kinase 3 β (GSK-3 β) inhibitors: thiadiazolidinones (TDZD) as potential drugs for the treatment of Alzheimer's disease. *J. Med. Chem.* 45, 1292–1299.

- (30) Martinez, A., Perez, D. I., and Gil, C. (2013) Lessons learnt from glycogen synthase kinase 3 inhibitors development for Alzheimer's disease. *Curr. Top. Med. Chem.* 13, 1808–1819.
- (31) Dinkova-Kostova, A. T., and Talalay, P. (2008) Direct and indirect antioxidant properties of inducers of cytoprotective proteins. *Mol. Nutr. Food Res.* 52 (Suppl 1), S128–138.
- (32) Gu, F., Chauhan, V., and Chauhan, A. (2015) Glutathione redox imbalance in brain disorders. *Curr. Opin. Clin. Nutr. Metab. Care* 18, 89–95.
- (33) Klein, W. L., Krafft, G. A., and Finch, C. E. (2001) Targeting small Abeta oligomers: the solution to an Alzheimer's disease conundrum? *Trends Neurosci.* 24, 219–224.
- (34) Simola, N., Morelli, M., and Carta, A. R. (2007) The 6-hydroxydopamine model of Parkinson's disease. *Neurotoxic. Res.* 11, 151–167.
- (35) Nass, R., Miller, D. M., and Blakely, R. D. (2001) C. elegans: a novel pharmacogenetic model to study Parkinson's disease. *Parkinsonism Relat Disord.* 7, 185–191.
- (36) Nass, R., Hahn, M. K., Jessen, T., McDonald, P. W., Carvelli, L., and Blakely, R. D. (2005) A genetic screen in Caenorhabditis elegans for dopamine neuron insensitivity to 6-hydroxydopamine identifies dopamine transporter mutants impacting transporter biosynthesis and trafficking. *J. Neurochem.* 94, 774–785.
- (37) (a) Illiano, P., Lanzo, A., Leo, D., Paglione, M., Zampi, G., Gainetdinov, R. R., and Di Schiavi, E. (2017) A Caenorhabditis elegans model to study dopamine transporter deficiency syndrome. *Eur. J. Neurosci.* 45, 207–214. (b) Nass, R., Hall, D. H., Miller, D. M., 3rd, and Blakely, R. D. (2002) Neurotoxin-induced degeneration of dopamine neurons in Caenorhabditis elegans. *Proc. Natl. Acad. Sci. U. S. A.* 99, 3264–3269.
- (38) An, J. H., Vranas, K., Lucke, M., Inoue, H., Hisamoto, N., Matsumoto, K., and Blackwell, T. K. (2005) Regulation of the Caenorhabditis elegans oxidative stress defense protein SKN-1 by glycogen synthase kinase-3. *Proc. Natl. Acad. Sci. U. S. A.* 102, 16275–16280.
- (39) Cardoso, F. L., Brites, D., and Brito, M. A. (2010) Looking at the blood-brain barrier: molecular anatomy and possible investigation approaches. *Brain Res. Rev.* 64, 328–363.
- (40) Di, L., Kerns, E. H., Fan, K., McConnell, O. J., and Carter, G. T. (2003) High throughput artificial membrane permeability assay for blood-brain barrier. *Eur. J. Med. Chem.* 38, 223–332.
- (41) Crivori, P., Cruciani, G., Carrupt, P. A., and Testa, B. (2000) Predicting blood-brain barrier permeation from three-dimensional molecular structure. *J. Med. Chem.* 43, 2204–2216.
- (42) ADP-Glo Kinase Assay Technical Manual. <https://www.promega.es/resources/protocols/technical-manuals/0/adp-glo-kinase-assay-protocol/> (2019-10-22).
- (43) Dias, K. S., de Paula, C. T., Dos Santos, T., Souza, I. N., Boni, M. S., Guimaraes, M. J., da Silva, F. M., Castro, N. G., Neves, G. A., Veloso, C. C., Coelho, M. M., de Melo, I. S., Giusti, F. C., Giusti-Paiva, A., da Silva, M. L., Dardenne, L. E., Guedes, I. A., Pruccoli, L., Morroni, F., Tarozzi, A., and Viegas, C., Jr. (2017) Design, synthesis and evaluation of novel feruloyl-donepezil hybrids as potential multitarget drugs for the treatment of Alzheimer's disease. *Eur. J. Med. Chem.* 130, 440–457.
- (44) Rampa, A., Montanari, S., Pruccoli, L., Bartolini, M., Falchi, F., Feoli, A., Cavalli, A., Belluti, F., Gobbi, S., Tarozzi, A., and Bisi, A. (2017) Chalcone-based carbamates for Alzheimer's disease treatment. *Future Med. Chem.* 9, 749–764.
- (45) Tarozzi, A., Bartolini, M., Piazzi, L., Valgimigli, L., Amorati, R., Bolondi, C., Djemil, A., Mancini, F., Andrisano, V., and Rampa, A. (2014) From the dual function lead AP2238 to AP2469, a multi-target-directed ligand for the treatment of Alzheimer's disease. *Pharmacol. Res. Perspect.* 2, No. e00023.
- (46) Dias Viegas, F. P., de Freitas Silva, M., Divino da Rocha, M., Castelli, M. R., Riquiel, M. M., Machado, R. P., Vaz, S. M., Simoes de Lima, L. M., Mancini, K. C., Marques de Oliveira, P. C., Moraes, E. P., Gontijo, V. S., da Silva, F. M. R., D'Alincourt da Fonseca Pecanha, D., Castro, N. G., Neves, G. A., Giusti-Paiva, A., Vilela, F. C., Orlandi, L., Camps, I., Veloso, M. P., Leomil Coelho, L. F., Ionta, M., Ferreira-Silva, G. A., Pereira, R. M., Dardenne, L. E., Guedes, I. A., de Oliveira Carneiro Junior, W., Quaglio Bellozi, P. M., Pinheiro de Oliveira, A. C., Ferreira, F. F., Pruccoli, L., Tarozzi, A., and Viegas, C., Jr. (2018) Design, synthesis and pharmacological evaluation of N-benzyl-piperidinyl-aryl-acylhydrazone derivatives as donepezil hybrids: Discovery of novel multi-target anti-alzheimer prototype drug candidates. *Eur. J. Med. Chem.* 147, 48–65.
- (47) Morroni, F., Sita, G., Djemil, A., D'Amico, M., Pruccoli, L., Cantelli-Forti, G., Hrelia, P., and Tarozzi, A. (2018) Comparison of Adaptive Neuroprotective Mechanisms of Sulforaphane and its Interconversion Product Erucin in in Vitro and in Vivo Models of Parkinson's Disease. *J. Agric. Food Chem.* 66, 856–865.
- (48) Brenner, S. (1974) The genetics of Caenorhabditis elegans. *Genetics.* 77, 71–94.
- (49) Marvanova, M., and Nichols, C. D. (2007) Identification of neuroprotective compounds of caenorhabditis elegans dopaminergic neurons against 6-OHDA. *J. Mol. Neurosci.* 31, 127–137.